The Molecular Basis for Attractive Salt-Taste Coding in *Drosophila*

Yali V. Zhang,[2] Jinfei Ni,[2] Craig Montell[1,2]*

Below a certain level, table salt (NaCl) is beneficial for animals, whereas excessive salt is harmful. However, it remains unclear how low- and high-salt taste perceptions are differentially encoded. We identified a salt-taste coding mechanism in *Drosophila melanogaster*. Flies use distinct types of gustatory receptor neurons (GRNs) to respond to different concentrations of salt. We demonstrated that a member of the newly discovered ionotropic glutamate receptor (IR) family, IR76b, functioned in the detection of low salt and was a Na^+ channel. The loss of IR76b selectively impaired the attractive pathway, leaving salt-aversive GRNs unaffected. Consequently, low salt became aversive. Our work demonstrated that the opposing behavioral responses to low and high salt were determined largely by an elegant bimodal switch system operating in GRNs.

To address the fundamental question of how low- and high-salt taste perceptions are differentially encoded in gustatory receptor neurons (GRNs) in insects, we chose the fruit fly as a model. We first tested the animal's behavioral responses to different salt concentrations ranging from 1 to 1000 mM, using a robust, food-color–based preference assay (fig. S1, A and B). Akin to mammals, flies preferred low-salt food (1 to 100 mM), with a maximal preference at 50 mM NaCl, whereas they rejected high-salt food (≥200 mM) (Fig. 1A) (*1*–*3*). This pattern differs from both sugar and bitter taste in that flies prefer sweet and dislike bitter compounds regardless of the concentration.

In *Drosophila*, the primary taste sensory organ, the labelum, contains 31 sensilla, which are further classified by size as small (S), intermediate (I), and large (L) sensilla (Fig. 1B) (*4*). Sensilla contain multiple GRNs, which respond to distinct stimuli, including bitter, sweet, and salty tastants (*4*–*6*). We surveyed the physiological responses of sensilla to low salt (50 mM) and high salt (500 mM) by performing tip recordings (*7*) (fig. S2). The GRNs housed by two L-type sensilla (L4 and L6) produced the most robust firings in response to low salt, whereas the GRNs in three S-type sensilla (S4, S6, and S8) displayed the strongest responses to high salt (fig. S2, A

[1]Neuroscience Research Institute and Department of Molecular, Cellular and Developmental Biology, University of California Santa Barbara, Santa Barbara, CA, 93110, USA. [2]Department of Biological Chemistry and Department of Neuroscience, The Johns Hopkins University School of Medicine, Baltimore, MD 21205, USA.

*Corresponding author. E-mail: craig.montell@lifesci.ucsb.edu

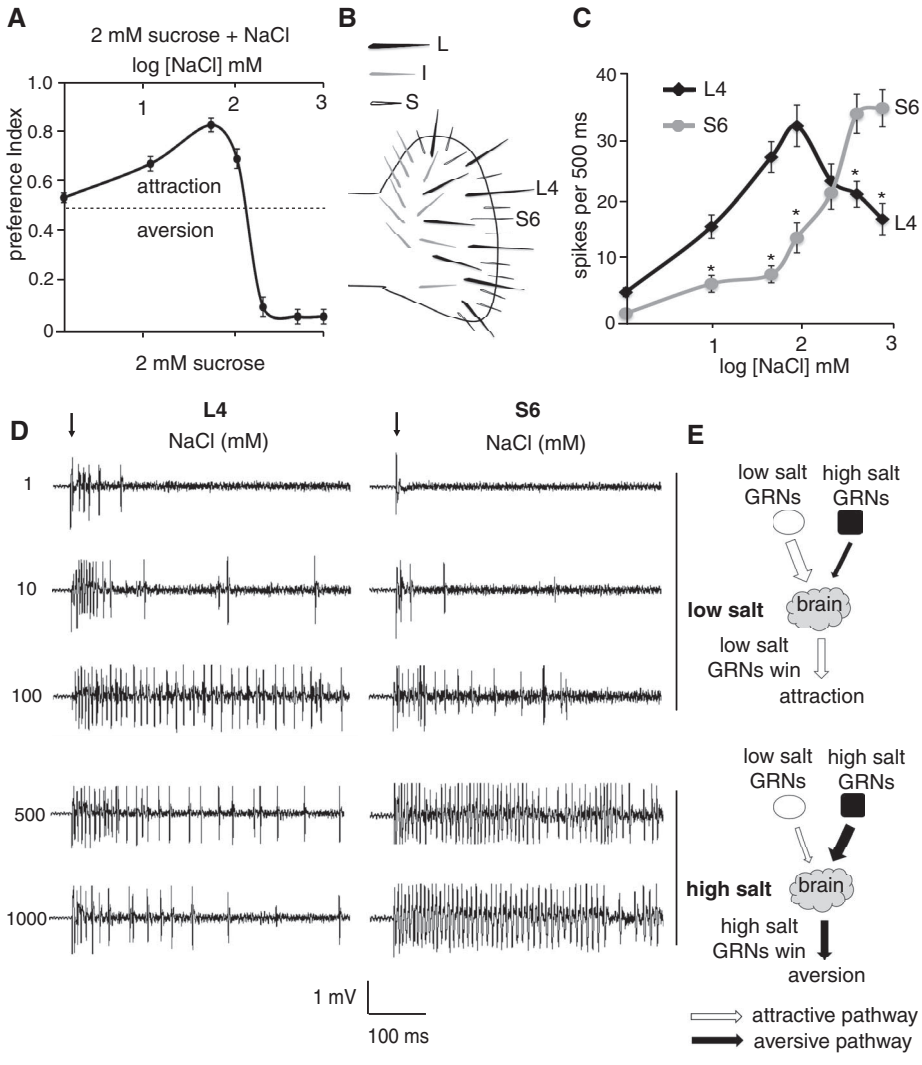

Fig. 1. Wild-type responses to different concentrations of salt. (**A**) Behavioral responses to 1 to 1000 mM salt. The dashed line indicates no preference. $n = 10$ trials with ~70 flies per trial. (**B**) Cartoon showing the distribution of L-, I-, and S-type sensilla in the labelum. (**C** and **D**) Tip recordings using L4 and S6 sensilla in response to low salt. $n = 10$. The arrows indicate application of the recording electrode to the sensilla. Error bars indicate SEMs; $^*P < 0.01$. (**E**) Schematic depicting how the L- and S-type sensilla differentially mediated attractive and aversive salt taste.

and C). These three S-type sensilla respond differentially to bitter tastants (*8*), suggesting that each type of gustatory sensillum has a unique taste tuning profile. GRNs in I-type sensilla responded to salt (*9*), but none as robustly as the most sensitive L- or S-type sensilla (fig. S2). With the exception of S4 and S8, the S-type sensilla show robust responses to the broadest array of aversive tastants (*5*, *8*), whereas L-type sensilla produce the strongest physiological responses to attractive tastants, such as sugars (*6*, *8*, *10*, *11*). Thus, we deduced that the responses to low and high salt (*5*, *6*, *12*) were likely to be controlled by a balance between the GRNs housed in L- and S-type sensilla.

We focused on L4 and S6 sensilla, using NaCl concentrations ranging from 1 to 1000 mM (Fig. 1, C and D). The firing of salt GRNs in the L4 sensilla increased progressively at low concentrations and peaked at 100 mM. In contrast, the salt GRNs in S6 sensilla were much less active than the salt GRNs in L4 sensilla, suggesting that these latter sensilla played a predominant role in low salt response. As the salt concentration increased above 100 mM, the firing of salt GRNs in L4 sensilla gradually declined. In contrast, the action potentials produced by S6 salt GRNs exhibited a remarkable increase (≥100 mM), with a maximal response at 500 mM. At high salt concentrations, the firing of S6 salt GRNs far exceeded that of L4 salt GRNs, indicating that the high-salt response was controlled predominantly by salt GRNs in S-type sensilla.

We therefore propose a model in which competition between GRNs in the S- and L-type sensilla accounts for the bidirectional behavioral responses to salt. At low concentrations, the low-salt GRNs dominate over the high-salt GRNs, thereby causing the animals to prefer low salt (Fig. 1E). At high salt levels, the high-salt GRNs overwhelm the low-salt GRNs, resulting in salt rejection.

We next tested several candidate salt receptors and channels, none of which affected salt taste (supplementary text). Ionotropic receptors (IRs) are a class of olfactory receptors in *Drosophila* that are distantly related to mammalian ionotropic glutamate receptors (iGluRs) (*13*). Several *Ir* genes, such as *Ir25a and Ir76b*, also appear to be expressed in gustatory sensilla (*13*–*15*). The $Ir25a^2$ mutant had no obvious deficits in sensing either low salt or high salt (fig S3, A and C). We then carried out a genetic analysis of *Ir76b* and generated two null alleles, $Ir76b^1$ and $Ir76b^2$, by P-element–mediated imprecise excision (Fig. 2A). We also retained a revertant line that underwent a precise P-element excision ($Ir76b^{R1}$). Loss of *Ir76b* did not impair the responses to potassium chloride, sucrose, water, or bitter tastants (fig. S4, A to C).

The *Ir76b* deletions resulted in severe defects in the attraction to low salt concentrations (1 to 100 mM; Fig. 2B). In contrast, the *Ir76b* mutants showed the same aversion to high salt as the $Ir76b^+$ control (w^{1118}). $Ir76b^{R1}$ behavior was indistinguishable from the wild-type $Ir76b^+$ control (w^{1118}) at all salt concentrations (Fig. 2B).

We next performed tip recordings to monitor physiological abnormalities in the GRNs. The *Ir76b* mutations caused a decrease in the number of action potentials by salt GRNs in L4 sensilla in response to 50 mM salt (Fig. 2, C and D), demonstrating a functional defect in the GRNs. There were no significant changes in the firing frequencies of S6 GRNs in the *Ir76b* mutants, as compared with the wild type (Fig. 2, C and D). Using the *Ir76b-Gal4* and *UAS-Ir76b* transgenes, we restored normal attractive responses to low salt in the $Ir76b^1$ mutant (Fig. 2, C to E).

We also examined the physiological responses to different salt concentrations (1 to 1000 mM NaCl). Loss of *Ir76b* caused significant reductions in the firing frequencies of the salt GRNs in L4 sensilla at all salt concentrations (Fig. 2E). The firing of salt GRNs in L6 sensilla was also impaired (fig. S4D). However, there were no effects on the physiological responses of

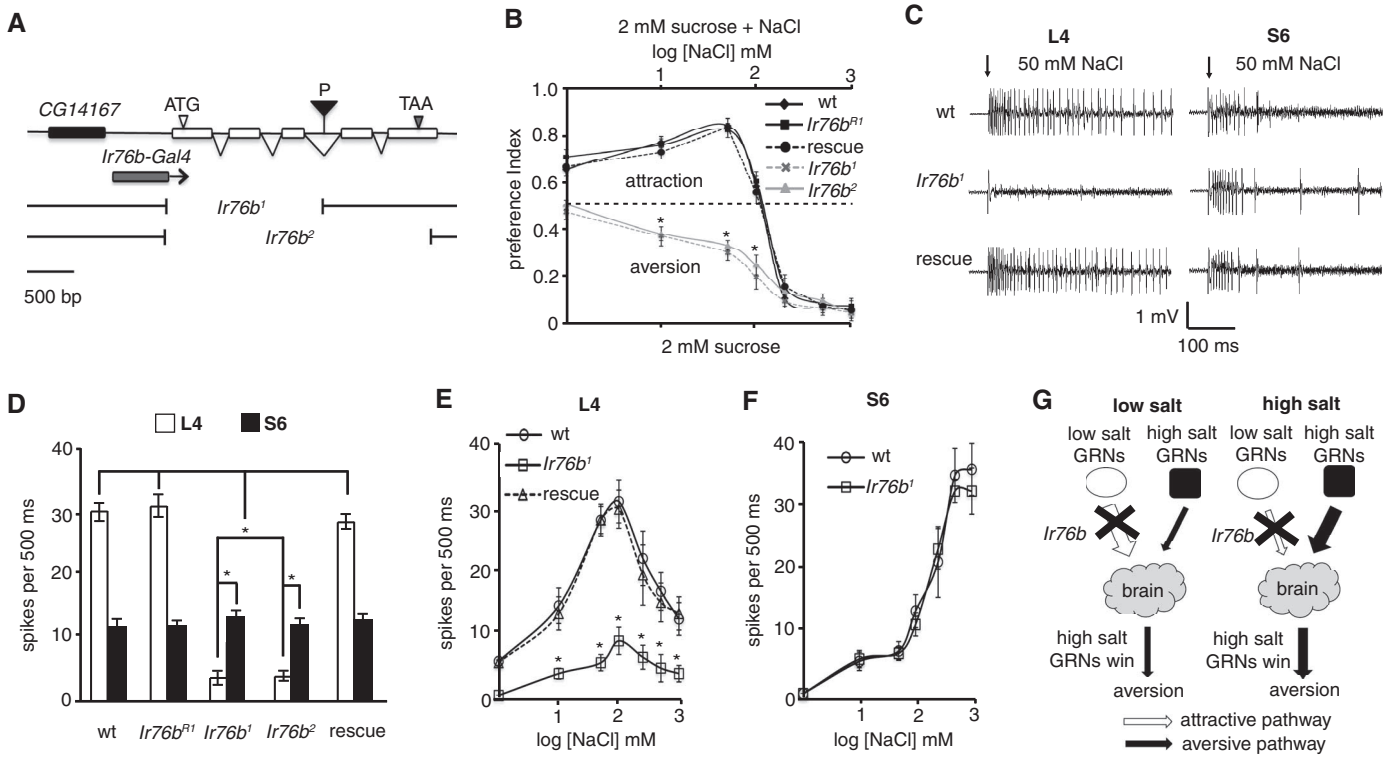

Fig. 2. *Ir76b* is required for low-salt preference. (**A**) Genomic organization of *Ir76b.* Shown are a P element (P) inserted in *Ir76b*, the deletions in $Ir76b^1$ and $Ir76b^2$, and the genomic region included in the *Ir76b-Gal4* transgene. (**B**) Two-way choice tests of sucrose versus sucrose plus salt. The rescue flies were $Ir76b^1$ flies harboring the *UAS-Ir76b* and the *Ir76b-Gal4* transgenes. $n = 10$. (**C** and **D**) 50 mM NaCl-induced action potentials in L4 and S6 sensilla. $n = 15$. (**E** and **F**) Action potential frequencies produced by L4 ($n = 5$) and S6 ($n = 3$) sensilla across different NaCl concentrations. Analysis of variance tests were performed. (**G**) Cartoon showing that the loss of *Ir76b* selectively disrupted the attractive salt taste pathway. Error bars indicate SEMs; $^*P < 0.01$.

high-salt GRNs in S4 or S6 sensilla (Fig. 2F and fig. S4E).

Taken together, our studies indicated that the removal of *Ir76b* selectively disrupted the attractive salt pathway, while leaving the aversive salt pathway intact (Fig. 2G). Consequently, *Ir76b* mutant animals avoided rather than preferred low salt, whereas they retained aversion to high salt.

To examine the cellular distribution pattern of IR76b, we raised antibodies against IR76b. The antibodies marked GRNs in the labellum, and the staining was virtually eliminated in *Ir76b* mutants (Fig. 3, A and B, and fig. S5A). We also generated flies expressing an *Ir76b* reporter (*Ir76b-Gal4*). In combination with *UAS-mCD8::GFP* or *UAS-dsRed*, we detected prominent GRN staining in the proboscis (Fig. 3, C and D). *Ir76b*-expressing GRNs were housed in all L-type sensilla, including L4 and L6 (Fig. 3C). We also detected *Ir76b* reporter expression in GRNs in the leg tarsi and wing margins, which sent projections to the ventral nerve cord (fig. S5, E to G). *Ir76b* reporter expression largely overlapped with the anti-IR76b staining, suggesting that the reporter reflected the bona fide cellular distribution of *Ir76b* (fig. S5, B to D).

To determine whether *Ir76b*-positive GRNs overlapped with *Gr66a*-expressing bitter-responsive or *Gr5a*-expressing sugar-responsive GRNs, we generated an *Ir76b* reporter using the Q system (*Ir76b-QF*) (*16*). Double labeling showed that *Ir76b*-positive GRNs were distinct from either *Gr66a* or *Gr5a* GRNs (Fig. 3, E and F). *Gr66a*- and *Gr5a*-positive GRNs project their axons from the labellum to non-overlapping portions of the subesophageal ganglion (SOG) in the brain (*17*, *18*). The projections of *Ir76b* GRNs in the SOG (Fig. 3G and fig. S5H) showed minimal overlap with regions innervated by the axons of *Gr5a* and *Gr66a* GRNs (Fig. 3, H and I). Thus, *Ir76b* GRNs represented a class of GRNs distinct from sugar- or bitter-responsive GRNs.

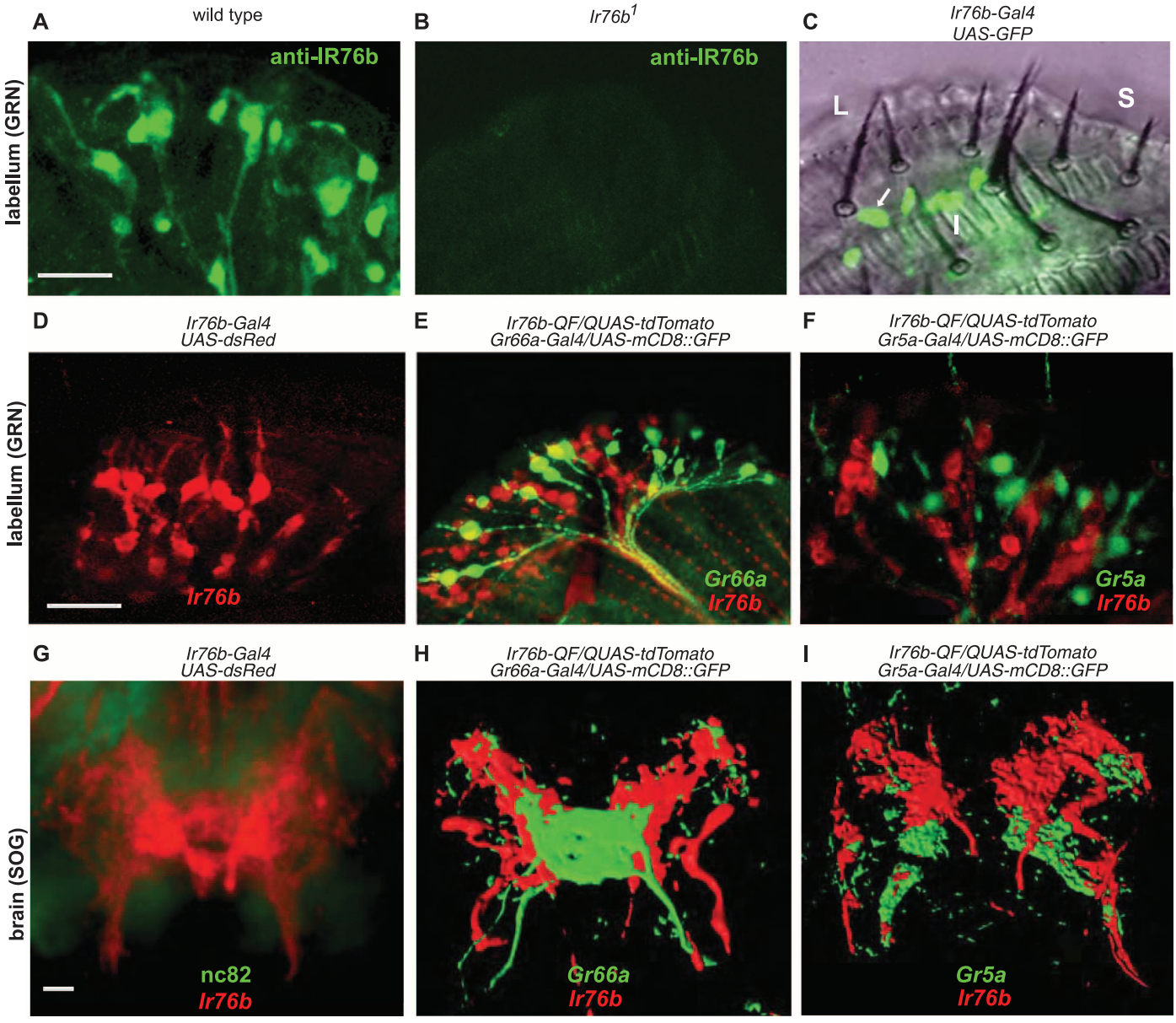

Fig. 3. Expression of *Ir76b* in GRNs. (**A** and **B**) Anti-IR76b staining of wild-type and *Ir76b*^{1} labela. (**C**) Green fluorescent protein (GFP) fluorescence superimposed on a bright-field view of a *Ir76b-Gal4/UAS-mCD8::GFP* labellum. The arrow indicates a GFP-positive GRN within an L4 sensillum. (**D**) *Ir76b* reporter staining a labellum. (**E**) Labellum expressing *Ir76b* (red) and *Gr66a* (green) reporters. (**F**) Labellum expressing *Ir76b* (red) and *Gr5a* (green) reporters. (**G**) Projections of GRNs in the SOG expressing an *Ir76b* reporter. (**H** and **I**) Three-dimensional reconstructions of the GRN projections in the SOG, using flies expressing *Ir76b* (red), *Gr66a* (green), and *Gr5a* (green) reporters as indicated. Scale bars, 10 μm.

In olfactory receptor neurons (ORNs), IRs function either alone or in conjugation with other IRs (*13*, *19*). We tested whether misexpression of IR76b alone conferred salt taste when introduced in non–salt-responsive GRNs. Because *Ir76b* and *Gr5a* are expressed in different GRN populations, we introduced *Ir76b* in *Gr5a*-sugar neurons in an *Ir76b*^{1} background. We recorded from L2 sensilla, which showed few responses to low salt even in the wild type (Fig. 4A). In response to NaCl, there was a robust train of action potentials produced by these *Gr5a* GRNs in L2 sensilla (Fig. 4, A and B, and fig. S6A). In contrast, these same GRNs did not induce a response to NMDGCl or potentiate the response to sucrose (Fig. 4, A and B). Thus, the action potentials were due to Na^+ and not Cl^- and were not a consequence of nonspecific elevation of *Gr5a* GRN activity. The behavioral deficit in low-salt preference in *Ir76b* mutants was rescued by misexpressing *Ir76b* in *Gr5a* GRNs (Fig. 4C).

To test whether IR76b was capable of functioning as a Na^+-permeable channel, we performed whole-cell recordings after expressing IR76b in HEK293T cells (fig. S7, A and B). The IR76b-expressing cells showed increased current (I_{IR76b}) relative to control cells (Fig. 4D). The nearly linear current-voltage (*I-V*) relationship indicated that I_{IR76b} was not strongly voltage-dependent (Fig. 4E). Replacement of the external Cl^- with gluconate anions had little effect on I_{IR76b} (fig. S7D). Using bionic conditions, the relative ion selectivity of IR76b was P_{Na} (1.0) = P_{Cs} (1.0) > P_K (0.4) (Fig. 4E and fig. S7, C and E). The Na^+ conductance properties of IR76b were similar to those of NALCN, a mouse Na^+ leak channel (*20*), and suggested that IR76b was in a constitutively open state.

The ion conductance of iGluRs is controlled by residues in the third transmembrane (TM3) region that includes YTANLAAFLT (*21*). In the absence of ligand, the channels are closed. A spontaneous A288T mutation in TM3 of mouse GluRδ2 (Lurcher mutation; GluRδ2^{Lc}) disrupts the closed conformation, resulting in a constitutive Na^+ conductance (*22*). IR76b harbored a threonine (T293) in nearly the same position as the Lurcher substitution (A288T; Fig. 4F and fig. S7, F and G). A threonine is absent in corresponding positions of other fly IRs and mammalian iGluRs (Fig, 4F). Therefore, we postulated that T293 enabled IR76b to be fixed in an open Na^+-permeable state. To test this idea, we replaced IR76b with IR76b^{T293A} and determined the effects of this substitution in vivo and in vitro. When expressing *UAS-Ir76b*^{T293A} using *Gr5a-Gal4*, we did not detect a salt response in L2 sensilla (Fig. 4A). Moreover, the T293A mutation greatly attenuated the constitutive current in HEK293T cells (Fig. 4, D and E).

To explain how the fly uses IR76b to detect salt, we propose that IR76b is a Na^+ leak channel and is effective because of the unusual extracellular cation composition bathing the GRNs. Different from the body hemolymph, which contains high Na^+, the endolymph that bathes insect chemosensory neurons appears to have a low Na^+ concentration (*23*). Under resting conditions, there may be little Na^+ conductance. After consuming Na^+-containing foods, the Na^+ levels in the endolymph rise, driving Na^+ influx through IR76b. The excitation of salt-attractive GRNs induces the animals to consume salt. Loss of IR76b selectively impaired the attractive pathway, making the otherwise attractive low salt become aversive.

Our work establishes that the salt attractive pathway relies on a type of Na^+-permeable channel not previously known to function in taste, and this channel, IR76b, bears no relationship to epithelial sodium channels (ENaCs) that are required for sensing low salt in mice (*24*). Some ENaC channels may be constitutively active (*25*) and lead to the depolarization of taste receptor cells after a rise in cation levels at the cell surface (*26*). Thus, despite the divergence between fly IRs and mammalian ENaC channels, they may mediate salt taste through similar mech-

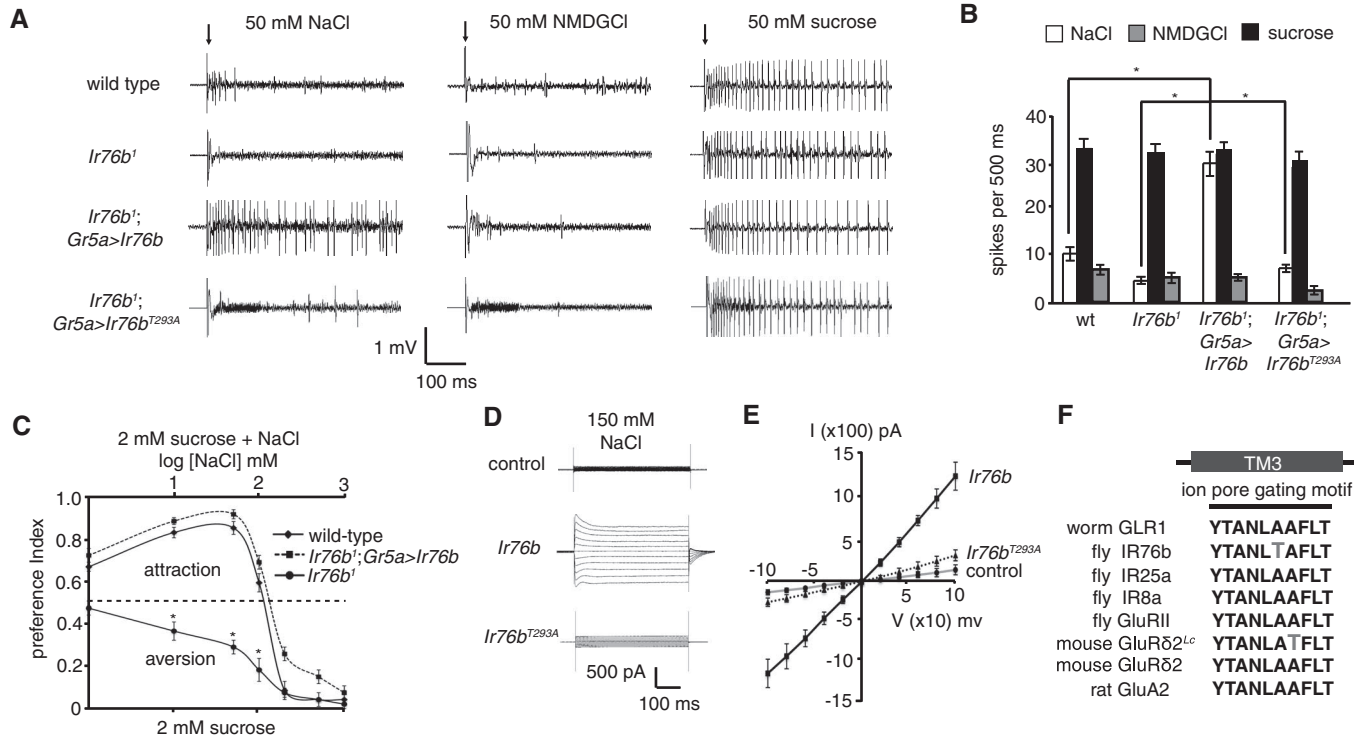

Fig. 4. *Ir76b* was sufficient to function as a salt sensor. (**A** and **B**) Tip recordings and quantification showing action potentials triggered by 50 mM NaCl after misexpression of *Ir76b* in *Gr5a* GRNs. NMDGCl and sucrose were negative and positive controls, respectively. $n = 10$. (**C**) Two-way choice tests (2 mM sucrose versus 2 mM sucrose plus different concentrations of NaCl) after misexpression of *UAS-Ir76b* using *Gr5a-Gal4*. $n = 5$. (**D**) Whole-cell voltage clamp recordings of HEK293T cells expressing wild-type IR76b or IR76b^{T293A} (with 150 mM NaCl in the bath). The cells were stimulated with voltage steps of 500 ms duration (–100 mV to +100 mV in 10-mV increments). (**E**) *I-V* relationships of cells expressing IR76b or IR76b^{T293A} (with 150 mM NaCl in the bath). Error bars indicate SEMs; *$P < 0.01$. (**F**) Sequences of the ion pore gating motif in TM3 of the indicated iGluRs and IRs.

anisms. Our competition model for low- and high-salt taste detection may represent a widely used mechanism for salt-taste coding in other animals, including mammals.

References and Notes

1. M. Nakamura, D. Baldwin, S. Hannaford, J. Palka, C. Montell, *J. Neurosci.* **22**, 3463 (2002).
2. R. Balakrishnan, V. Rodrigues, *J. Exp. Biol.* **157**, 161 (1991).
3. L. Liu *et al.*, *Neuron* **39**, 133 (2003).
4. S. R. Shanbhag, S. K. Park, C. W. Pikielny, R. A. Steinbrecht, *Cell Tissue Res.* **304**, 423 (2001).
5. M. Hiroi, N. Meunier, F. Marion-Poll, T. Tanimura, *J. Neurobiol.* **61**, 333 (2004).
6. L. B. Vosshall, R. F. Stocker, *Annu. Rev. Neurosci.* **30**, 505 (2007).
7. E. S. Hodgson, J. Y. Lettvin, K. D. Roeder, *Science* **122**, 417 (1955).
8. L. A. Weiss, A. Dahanukar, J. Y. Kwon, D. Banerjee, J. R. Carlson, *Neuron* **69**, 258 (2011).
9. N. Meunier, F. Marion-Poll, J. P. Rospars, T. Tanimura, *J. Neurobiol.* **56**, 139 (2003).
10. A. Dahanukar, Y. T. Lei, J. Y. Kwon, J. R. Carlson, *Neuron* **56**, 503 (2007).
11. C. Montell, *Curr. Opin. Neurobiol.* **19**, 345 (2009).
12. N. Fujishiro, H. Kijima, H. Morita, *J. Insect Physiol.* **30**, 317 (1984).
13. R. Benton, K. S. Vannice, C. Gomez-Diaz, L. B. Vosshall, *Cell* **136**, 149 (2009).
14. V. Croset *et al.*, *PLoS Genet.* **6**, e1001064 (2010).
15. P. Cameron, M. Hiroi, J. Ngai, K. Scott, *Nature* **465**, 91 (2010).
16. C. J. Potter, B. Tasic, E. V. Russler, L. Liang, L. Luo, *Cell* **141**, 536 (2010).
17. Z. Wang, A. Singhvi, P. Kong, K. Scott, *Cell* **117**, 981 (2004).
18. N. Thorne, C. Chromey, S. Bray, H. Amrein, *Curr. Biol.* **14**, 1065 (2004).
19. L. Abuin *et al.*, *Neuron* **69**, 44 (2011).
20. B. Lu *et al.*, *Cell* **129**, 371 (2007).
21. A. I. Sobolevsky, M. P. Rosconi, E. Gouaux, *Nature* **462**, 745 (2009).
22. J. Zuo *et al.*, *Nature* **388**, 769 (1997).
23. K.-E. Kaissling, J. Thorson, in *Receptors for Neurotransmitters, Hormones, and Pheromones in Insects,* D. B. Sattelle, L. M. Hall, J. G. Hildebrand, Eds. (Elsevier, Amsterdam, 1980), pp. 261–282.
24. J. Chandrashekar *et al.*, *Nature* **464**, 297 (2010).
25. F. J. McDonald, M. P. Price, P. M. Snyder, M. J. Welsh, *Am. J. Physiol.* **268**, C1157 (1995).
26. J. A. DeSimone, G. L. Heck, S. K. DeSimone, *Science* **214**, 1039 (1981).

Acknowledgments: This project was supported by a grant to C.M. from the National Institute on Deafness and Other Communication Disorders (DC007864).

Supplementary Materials

www.sciencemag.org/cgi/content/full/340/6138/1334/DC1
Materials and Methods
Supplementary Text
Figs. S1 to S7
References

17 December 2012; accepted 2 April 2013
10.1126/science.1234133

Parallel Neural Pathways Mediate CO_2 Avoidance Responses in *Drosophila*

Hui-Hao Lin,[1] Li-An Chu,[1] Tsai-Feng Fu,[2] Barry J. Dickson,[3] Ann-Shyn Chiang[1,4,5,6]*

Different stimulus intensities elicit distinct perceptions, implying that input signals are either conveyed through an overlapping but distinct subpopulation of sensory neurons or channeled into divergent brain circuits according to intensity. In *Drosophila*, carbon dioxide (CO_2) is detected by a single type of olfactory sensory neuron, but information is conveyed to higher brain centers through second-order projection neurons (PNs). Two distinct pathways, PN_v-1 and PN_v-2, are necessary and sufficient for avoidance responses to low and high CO_2 concentrations, respectively. Whereas low concentrations activate PN_v-1, high concentrations activate both PN_vs and GABAergic PN_v-3, which may inhibit PN_v-1 pathway-mediated avoidance behavior. Channeling a sensory input into distinct neural pathways allows the perception of an odor to be further modulated by both stimulus intensity and context.

Insects detect odor with olfactory sensory neurons (OSNs), which converge to the antennal lobe (AL) before conveyance to the mushroom body (MB) and lateral horn (LH) via stereotyped projection neurons (PNs) (*1*–*4*). In *Drosophila*, carbon dioxide (CO_2) concentrations lower than 2% activate only one type of OSN that expresses *Gr21a* and *Gr63a* receptors and projects to a single V-glomerulus (*5*–*9*). We examined the morphology and functionality of PNs innervating the V-glomerulus (PN_vs) with regard to CO_2 responses.

We expressed a photoactivatable green fluorescent protein (PaGFP) in ~60% of neurons using *Cha-Gal4>UAS-PaGFP* flies (*10*–*12*) and labeled candidate PN_vs by means of targeted photoconversion (fig. S1A). Although nearby tracts could have been labeled, the circuits were complemented and validated by browsing single neuron representations in the FlyCircuit database (*13*). Up to 12 heteromorphic PN_vs with different morphologies may link the V-glomerulus and higher brain centers (figs. S1B and S2) via the inner, medial, and outer antennocerebral tracts (iACT, mACT, and oACT, respectively).

To assess the functional roles of these PN_vs, we identified 50 *Gal4* lines that labeled the V-glomerulus, including seven putative PN_vs. We used genetic mosaic analyses to resolve individual neurons, using either repressible cell marker (MARCM) (*14*), FLP-out (*2*), or *Brainbow* (fig. S3) techniques to identify four genetically addressable PN_vs: PN_v-1 (*VT33008-Gal4*, *VT1606-Gal4*, *VT31497-Gal4*, and *VT48643-Gal4*) (Fig. 1, A to D), which links the bilateral V-glomeruli via oACT to the lateral horn (LH) and calyx (Cal); PN_v-2 (*E0044-Gal4*) (Fig. 1E), which connects a single V-glomerulus via iACT to the bilateral superior dorsofrontal protocerebrum (SDFP); PN_v-3 (*VT12760-Gal4*) (Fig. 1F), which innervates all glomeruli of a single AL and projects via mACT to the LH, inner dorsolateral protocerebrum (IDLP), and SDFP; and PN_v-4 (*E0564-Gal4*) (Fig. 1G), which links two ALs via oACT to the SDFP, superpeduncular protocerebrum (SPP), caudal ventrolateral protocerebrum (CVLP), IDLP, and LH. Their termini are primarily localized to the SDFP and LH (fig. S4) (*13*).

Using Dscam[exon17.1]::GFP as a dendritic marker (*15*), we demonstrated that they all project into the V-glomerulus (Fig. 1, Ab–Gb). We used the GRASP (green fluorescent protein reconstitution across synaptic partners) technique to assess whether these dendrites receive input from CO_2 OSNs (*16*, *17*). Half of the split-GFP GRASP reporter was expressed in OSN_v neurons by using *L5131-LexA* (fig. S5Aa), which specifically labels OSNs (fig. S5Ab) that are *Gr21a-nlsDsRed*–positive (fig. S5B), innervate the V-glomerulus (fig. S5Ca), and respond to 0.5% CO_2 (fig. S5C, b and c). The other half was expressed in distinct PN_vs by using an appropriate *Gal4* driver. In all cases, GRASP signals were observed in the V-glomerulus (Fig. 1, Ac to Gc). In the control experiment using *Mz19-Gal4* expressed in PNs innervating several other glomeruli (fig. S5D), GRASP signals were absent in the V-glomerulus (fig. S5E).

Monitoring functional responses in the V-glomerulus with a genetically encoded calcium indicator (GCaMP) revealed that all four PN_v types responded to CO_2 but not air, methylcyclohexanol (MCH), or octanol (OCT). PN_v-1 and PN_v-4 responded equally to 0.5 and 2% CO_2, whereas PN_v-2 and PN_v-3 responded dose-dependently (Fig. 1, Ae to Ge). Quantitative fluorescence measurement showed that basal GCaMP expression driven by seven *PN_v-Gal4* lines varied more than twofold (fig. S6A). A functional curve to different CO_2 concentrations showed that CO_2-

[1]Institute of Biotechnology, National Tsing Hua University, Hsinchu 30013, Taiwan. [2]Department of Applied Chemistry, National Chi Nan University, University Road, Puli, Nantou 545, Taiwan. [3]Research Institute of Molecular Pathology, Dr Bohr-Gasse 7, A-1030 Vienna, Austria. [4]Brain Research Center, National Tsing Hua University, Hsinchu 30013, Taiwan. [5]Genomics Research Center, Academia Sinica, Nankang, Taipei 115, Taiwan. [6]Kavli Institute for Brain and Mind, University of California at San Diego, La Jolla, CA 92093–0526, USA.

*Corresponding author. E-mail: aschiang@life.nthu.edu.tw

The Molecular Basis for Attractive Salt-Taste Coding in *Drosophila*

Yali V. Zhang *et al.*

Science **340**, 1334 (2013);
DOI: 10.1126/science.1234133